Chiral plasmons without magnetic field

Justin C. W. Song[a,b,c,1] and Mark S. Rudner[d]

[a]Walter Burke Institute of Theoretical Physics, California Institute of Technology, Pasadena, CA 91125; [b]Institute of Quantum Information and Matter, California Institute of Technology, Pasadena, CA 91125; [c]Department of Physics, California Institute of Technology, Pasadena, CA 91125; and [d]Center for Quantum Devices and Niels Bohr International Academy, Niels Bohr Institute, University of Copenhagen, 2100 Copenhagen, Denmark

Edited by Allan H MacDonald, The University of Texas at Austin, Austin, TX, and approved February 19, 2016 (received for review September 24, 2015)

Plasmons, the collective oscillations of interacting electrons, possess emergent properties that dramatically alter the optical response of metals. We predict the existence of a new class of plasmons—chiral Berry plasmons (CBPs)—for a wide range of 2D metallic systems including gapped Dirac materials. As we show, in these materials the interplay between Berry curvature and electron–electron interactions yields chiral plasmonic modes at zero magnetic field. The CBP modes are confined to system boundaries, even in the absence of topological edge states, with chirality manifested in split energy dispersions for oppositely directed plasmon waves. We unveil a rich CBP phenomenology and propose setups for realizing them, including in anomalous Hall metals and optically pumped 2D Dirac materials. Realization of CBPs will offer a powerful paradigm for magnetic field-free, subwavelength optical nonreciprocity, in the mid-IR to terahertz range, with tunable splittings as large as tens of THz, as well as sensitive all-optical diagnostics of topological bands.

topological materials | interactions | nonreciprocal response | Berry curvature

In electronic systems, chirality expresses the system's ability to discriminate between forward and backward propagation of electronic signals along certain directions. This technologically useful and hotly sought-after property can be achieved through the application of external magnetic fields. However, the need for strong applied fields "on-chip" brings many challenges for applications. Recently, materials exhibiting chirality in the absence of a magnetic field have started to gain prominence. These materials include metals exhibiting anomalous (1) and quantum anomalous (2–6) Hall effects, as well as nonmagnetic materials pushed out of equilibrium, where, for example, a zero-field charge Hall effect was recently demonstrated (7). In each case, zero-field chirality arises from Bloch band Berry curvature, a fundamental property of Bloch eigenstates that dramatically affects single-particle electronic motion and material responses (1, 8, 9).

Here we show that Berry curvature can work in concert with interactions, leading to new types of collective modes in 2D topological metals, with nonvanishing Berry flux (i.e., net Berry curvature), $\mathcal{F}$. In particular, $\mathcal{F}$ gives rise to chiral plasmonic excitations—propagating charge density waves with split dispersion for oppositely directed modes—in the absence of a magnetic field (Fig. 1). We refer to these collective modes as chiral Berry plasmons (CBPs). Notably, these chiral modes are localized to the edge of the 2D metal, even in the absence of topological edge states, and exhibit a rich phenomenology (see below).

We expect CBPs to be manifested in a wide variety of magnetic and nonmagnetic materials. The former are materials that exhibit anomalous Hall effects, wherein time reversal symmetry (TRS) breaking is encoded in the Bloch band Berry curvature. The latter include a range of readily available gapped Dirac materials, e.g., transition metal dichalcogenides and graphene/hBN, wherein TRS breaking is achieved by inducing a nonequilibrium valley polarization (7). In both cases CBPs are characterized by clear optical signatures such as split peaks in optical absorption.

From a technological perspective, CBPs in nonmagnetic materials are particularly appealing because they provide an entirely new platform for achieving a range of magneto-optical effect analogs that are magnetic field free and "on demand." A prime example is optical nonreciprocity (10), which is central for optical device components, e.g., optical isolators and circulators. Above a threshold frequency ($\omega_{\rm th}$; shaded area in Fig. 1*A*), the single unidirectionally propagating mode $\omega_{-}^{\rm edge}$ allows for chiral transport of light via coupling to CBPs. Such CBP-mediated waveguides provide a novel paradigm for deep subwavelength (11–13), linear, and magnetic field-free strong nonreciprocity, crucial for miniaturizing optical components. In particular, we predict that CBPs can enable nonreciprocity over a large technologically important bandwidth (terahertz to mid-IR).

The intrinsic chirality of CBPs starkly contrasts with that achieved via cyclotron motion of charged particles in a magnetic field, with important quantitative and qualitative consequences. In the latter case, chirality arises via the Lorentz force and gives rise to conventional magnetoplasmons (14–18). There, the cyclotron frequency, $\hbar\omega_c = \hbar eB/m$ (19–21), determines the constant splitting between magnetoplasmon modes of opposite chirality, which can be of the order of a few millielectron volts for accessible field strengths. In contrast, chirality in CBPs arises from the combined action of plasmonic self-generated electric fields and the anomalous velocity of Bloch electrons, the phase space dual to the Lorentz force. This combination makes the CBP mode splitting directly sensitive to plasmon wavelength, the Berry flux, and interaction strength, in contrast to magnetoplasmon splittings, which only depend on magnetic field (17, 22).[†] As a result, for short wavelengths and unscreened interactions, large splittings $\hbar\Delta\omega$ of several tens to a hundred millielectron volts can be achieved (Eq. **3**).

Self-Induced Anomalous Velocity

The origin of CBPs in two dimensions can be understood from the Euler equations for electron density, $n(\mathbf{r},t)$ (23)

Significance

A class of collective excitations is introduced, arising from the combined action of electron interactions and Berry curvature. These excitations manifest as chiral plasmonic modes at zero magnetic field. These collective modes are predicted to arise in a range of anomalous Hall metals, yielding a fundamental characteristic of interacting topological metals with non-zero Berry flux. Featuring a rich set of properties, these modes will enable versatile new tools for molding the flow of light.

Author contributions: J.C.W.S. and M.S.R. designed the research, performed the research, and wrote the paper.

The authors declare no conflict of interest.

This article is a PNAS Direct Submission.

[1]To whom correspondence should be addressed. Email: justin.song.cw@gmail.com.

This article contains supporting information online at www.pnas.org/lookup/suppl/doi:10.1073/pnas.1519086113/-/DCSupplemental.

[†]We note that Kohn's theorem guarantees that splittings are unchanged for parabolic bands; weak renormalizations are expected for linearly dispersing systems such as graphene, where it has been measured to be at most of order 10% (42). In contrast, for CBPs, the splitting grows directly proportional with interaction strength (Eq. **3**).

$$\partial_t n(\mathbf{r},t) + \nabla\cdot\bar{\mathbf{v}}(\mathbf{r},t) = 0, \quad [1a]$$

$$\partial_t \bar{\mathbf{p}}(\mathbf{r},t) - n(\mathbf{r},t)\, e\nabla\phi(\mathbf{r},t) = 0, \quad [1b]$$

where $\bar{\mathbf{v}}(\mathbf{r},t)$ and $\bar{\mathbf{p}}(\mathbf{r},t)$ are the velocity and momentum density fields, $\phi(\mathbf{r})$ is the scalar electric potential, and $-e<0$ is the electron charge. We note that in principle, the force equation, Eq. **1b**, also includes contributions arising from the stress density of the electronic fluid. However, at long-wavelengths these contributions yield only subleading corrections to the plasmon dispersion (24). As our aim here is to clearly and most simply demonstrate the existence and main features of CBPs, in this work we neglect small corrections due to the stress density. For an alternative formulation in terms of currents and conductivities, see *SI Appendix*.[‡]

To fully specify the dynamics, Eq. **1** must be supplemented by a set of constitutive relations that relate velocity, momentum, density, and the electric potential. Plasmons emerge from Eq. **1** as self-sustained collective oscillations of $n(\mathbf{r},t)$, with the potential $\phi(\mathbf{r},t) = \int d^2\mathbf{r}'\, W(\mathbf{r},\mathbf{r}')\delta n(\mathbf{r}',t)$ generated by the plasmon's density fluctuations $\delta n = n(\mathbf{r},t) - n_0$. Here n_0 is the average carrier density, and $W(\mathbf{r},\mathbf{r}')$ is the Coulomb interaction.

As we argue, in the presence of Berry curvature, the constitutive relations take on an anomalous character. The form of the constitutive relations can be found by starting with the quasiparticle semiclassical equations of motion (8), $\mathbf{v}_\mathbf{p} = \frac{\partial\varepsilon_\mathbf{p}}{\partial\mathbf{p}} + \frac{1}{\hbar}\dot{\mathbf{p}}\times\boldsymbol{\Omega}(\mathbf{p})$, $\dot{\mathbf{p}} = e\nabla\phi(\mathbf{r})$, where $\mathbf{v}_\mathbf{p} = \dot{\mathbf{r}}$ is the quasiparticle velocity and $\varepsilon_\mathbf{p}$ and $\boldsymbol{\Omega}(\mathbf{p}) = \Omega(\mathbf{p})\hat{\mathbf{z}}$ are the Bloch band dispersion and Berry curvature, respectively.[§] The corresponding velocity density fields are found from these relations and the phase space density $f_i(\mathbf{r},\mathbf{p},t)$ by summing over all momentum $\mathbf{p}$ and bands $\{i\}$, $\overline{\mathcal{O}}(\mathbf{r},t) = \sum_i \int d^2\mathbf{p}\, \mathcal{O} f_i(\mathbf{r},\mathbf{p},t)/(2\pi\hbar)^2$. This approach gives

$$\bar{\mathbf{v}}(\mathbf{r},t) = \frac{\bar{\mathbf{p}}(\mathbf{r},t)}{m} + \bar{\mathbf{v}}_a(\mathbf{r},t),\ \bar{\mathbf{v}}_a = \frac{e\mathcal{F}}{\hbar}[(\nabla\phi)\times\hat{\mathbf{z}}], \quad [2]$$

where $\mathcal{F} = \sum_i \int d^2\mathbf{p}\, \Omega_i(\mathbf{p}) f_i^0(\mathbf{p})/(2\pi\hbar)^2$ is the (dimensionless) Berry flux, with $f_i^0(\mathbf{p})$ being the equilibrium band occupancy; here, we have only kept terms linear in δn and $\nabla\phi$. In addition to the conventional first term, which governs the behavior of ordinary plasmons, $\bar{\mathbf{v}}(\mathbf{r},t)$ in Eq. **2** exhibits a self-induced anomalous velocity component $\bar{\mathbf{v}}_a$ that yields chirality as shown in Fig. 1. Note that the mass m appearing in Eq. **2** is the plasmon mass, which characterizes the collective motion of the Fermi sea (25).

CBP chirality can be understood intuitively by examining the anomalous velocity pattern set up by the plasmon's electrostatic potential ϕ (a more complete treatment is given below). Due to the cross-product in Eq. **2**, the anomalous velocity flow is directed along the equipotential contour lines of ϕ (see arrowheads in Fig. 1 *C* and *D*). Near an edge, surface charges associated with the plasmon wave produce a potential as shown in Fig. 1*D*. The corresponding anomalous velocity field directs electrons into the nodal regions to the left of each region of negative charge build up (i.e., excess electron density), for the orientation shown and $\mathcal{F}>0$. Thus, for a leftward direction of plasmon propagation, the anomalous velocity flow assists the collective motion of the electronic density wave, leading to faster propagation ω_+^{edge}. For the right-propagating mode, the anomalous flow works against the collective motion, yielding slower propagation ω_-^{edge}.

Crucially, $\bar{\mathbf{v}}_a$ depends directly on the self-generated electric field $-\nabla\phi(\mathbf{r})$. Consequently, the magnitude of the splitting is governed by the wave vector q and the strength of Coulomb interactions. We emphasize, however, that CBPs are a linear phenomenon, with the mode splitting $\Delta\omega$ independent of the magnitude of ϕ. As we will show, the q-dependent CBP splitting can be large

$$\hbar\Delta\omega = \hbar\left(\omega_+^{\text{edge}} - \omega_-^{\text{edge}}\right) \approx \mathcal{A}\frac{e^2}{\kappa}\mathcal{F}|q|, \quad [3]$$

where $\mathcal{A}$ is a numerical prefactor of order unity that depends on geometry, and we used the 2D Coulomb potential $W(\mathbf{q}) = 2\pi e/(\kappa|\mathbf{q}|)$ with background dielectric constant κ. For edge CBPs, we find $\mathcal{A} = 8\sqrt{2}\pi/9$ (see below), yielding large splittings $\hbar\Delta\omega \approx 6-60$ meV for $q = 1-10\ \mu\text{m}^{-1}$ (here we used $\mathcal{F}=1$, $\kappa=1$). The appearance of e^2/κ on the right side of Eq. **3** signals the crucial role interactions play in $\Delta\omega$.

Chiral Edge Berry Plasmons

We now analyze collective motion described by Eq. **1**, treating the electric potential ϕ self-consistently. For an infinite bulk, applying ∂_t to the continuity relation in Eq. **1a**, using Eq. **2**, and substituting in the force equation, Eq. **1b**, yields

$$-\partial_t^2\delta n = \frac{n_0 e}{m}\nabla^2\phi,\ \phi(\mathbf{r}) = \int_{-\infty}^{\infty} d\mathbf{r}'\, W(\mathbf{r}-\mathbf{r}')\delta n(\mathbf{r}'). \quad [4]$$

In arriving at Eq. **4**, we used $\nabla\cdot\bar{\mathbf{v}}_a \propto \partial_x\partial_y\phi(\mathbf{r}) - \partial_y\partial_x\phi(\mathbf{r}) = 0$. Importantly, Berry flux $\mathcal{F}$ is absent in Eq. **4** and has no effect on bulk plasmon dispersion. Indeed, decomposing into Fourier modes $\delta n \sim e^{i\omega t - i\mathbf{q}\cdot\mathbf{r}}$ and using the Coulomb interaction $W(\mathbf{r},\mathbf{r}') = -e/(\kappa|\mathbf{r}-\mathbf{r}'|)$ yields the usual 2D plasmon dispersion

$$\left(\hbar\omega_\mathbf{q}^{\text{bulk}}/\mu\right)^2 = a_0(q/q_0),\quad a_0 = \frac{2\pi\hbar^2}{m\mu}n_0,\quad q_0 = \frac{\kappa\mu}{e^2}, \quad [5]$$

which remains gapless at $q=0$. In contrast, bulk magnetoplasmons are gapped due to cyclotron motion (15–18).

Close to a boundary, the situation is dramatically altered: Berry flux $\mathcal{F}$ leads to the emergence of chiral edge plasmons, 1D chiral analogs of surface plasmons (20, 26). This behavior is most easily illustrated for an infinite metallic half-plane, where $n(\mathbf{r},t)$ and $\bar{\mathbf{v}}(\mathbf{r},t)$ are generically finite for $x\geq 0$, but are zero for $x<0$. Here the plasmon propagates as a plane wave along y, with the fields in Eq. **4** taking the form

$$\phi(\mathbf{r},t) = \phi_q(x)e^{i\omega t - iqy},\quad \delta n(\mathbf{r},t) = \delta n_q(x)e^{i\omega t - iqy}. \quad [6]$$

The presence of the edge allows charges to accumulate (Fig. 1*D*). Indeed, inserting the fields defined above into Eq. **1a** yields $\delta n(\mathbf{r})e^{i\omega t} = -\nabla\cdot[\bar{\mathbf{v}}(\mathbf{r},t)\Theta(x)]/i\omega$. Here we explicitly inserted $\Theta(x)$ to emphasize the vanishing of the velocity density outside the metallic half-plane [$\Theta(x)=1$ for $x\geq 0$ and $\Theta(x)=0$ for $x<0$]. Due to the $\Theta(x)$ inside the divergence above, a nonzero $\bar{\mathbf{v}}_x$ flowing into the boundary induces an oscillating surface charge component of $\delta n(\mathbf{r})e^{i\omega t}$ concentrated at the edge $x=0$ (26, 27). By replacing $\delta n(\mathbf{r},t)$ by $-\nabla\cdot[\bar{\mathbf{v}}(\mathbf{r},t)\Theta(x)]/i\omega$ in the integral for $\phi(\mathbf{r},t)$ in Eq. **4**, we thus find a jump condition for $\partial_x\phi_q(x)$ at $x=0$:

$$\partial_x\phi_q\big|_{0^+} - \partial_x\phi_q\big|_{0^-} = \frac{1}{i\omega}\left(\partial_x W_q\big|_{0^-} - \partial_x W_q\big|_{0^+}\right)\bar{\mathbf{v}}_x\big|_{0^+}, \quad [7]$$

where $W_q(x) = -(e/\kappa)\int_{-\infty}^{\infty} dk\, e^{ikx}/\left|q^2+k^2\right|^{1/2}$ is the 1D effective Coulomb interaction. Here we decomposed Eq. **4** into plane-waves using Eq. **6** and integrated across the delta function, $\partial_x\Theta(x) = \delta(x)$, which accounts for the surface charge layer. The

[‡]See *SI Appendix* for discussions of: an alternative formulation of CBPs based on current densities and the conductivity tensor, chiral Berry plasmon dipole modes in a disk, optical selection rules for gapped Dirac materials with inversion symmetry breaking, and photo-induced CBPs.

[§]The Berry curvature $\Omega(\mathbf{p}) = \nabla_\mathbf{k}\times\mathbf{A}_\mathbf{k}$ depends on the crystalline Bloch wavefunctions $|u_\mathbf{k}\rangle$, where $\mathbf{A}_\mathbf{k} = \langle u_\mathbf{k}|i\nabla_\mathbf{k}|u_\mathbf{k}\rangle$ is the Berry connection.

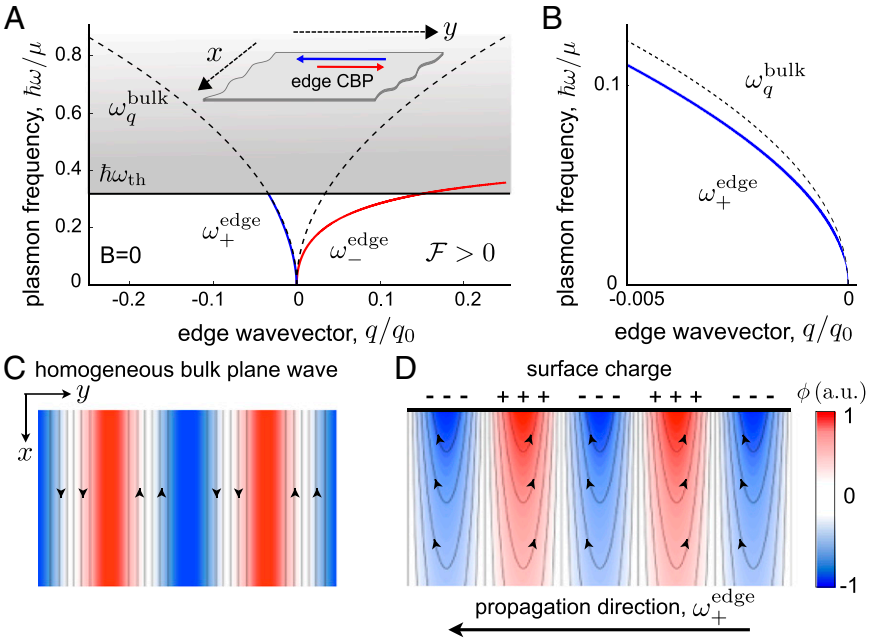

Fig. 1. CBPs at zero magnetic field. (*A*) CBPs are manifested along the edges of a 2D metal with nonvanishing Berry flux, $\mathcal{F}$ (*Inset*). Counterpropagating modes exhibit a split dispersion, $\omega_\pm^{\rm edge}(q)$, with the splitting increasing with wave vector q along the edge. Above a threshold frequency $\omega_{\rm th}$ (shaded region) the fast mode $\omega_+^{\rm edge}$ merges with bulk plasmon modes, $\omega_{\mathbf{q}}^{\rm bulk}$, see Eq. **5** and dashed line, leaving a single unidirectional mode $\omega_-^{\rm edge}$ propagating along the edge. (*B*) Zoom-in of *A* showing separation of $\omega_+^{\rm edge}$ and $\omega_{\mathbf{q}}^{\rm bulk}$ below $\omega_{\rm th}$. (*C* and *D*) Electric potential for bulk and edge plasmon modes. For bulk modes, the anomalous velocity field for electrons (indicated by arrowheads) runs parallel to the wave fronts and does not affect the speed of collective propagation. Near edges the buildup of surface charges leads to an anomalous velocity flow that assists the collective propagation for the $\omega_+^{\rm edge}$ mode (see text below Eq. **2**). For $\omega_-^{\rm edge}$, the anomalous velocity flow opposes the collective motion (see text below Eq. **2**). Parameter values used: $\mathcal{F}=1.0$ and $a_0=3$ for *A* and *B* (Eq. **5**) and $|q/q_0|=0.3$, $\mathcal{F}=0.3$, and $a_0=3$ for *C* and *D*.

parameter q corresponds to the wavevector in y (along the edge), and k describes variations in x (perpendicular to the edge). Crucially, finite $\mathcal{F}$ in Eq. **2** makes $\bar{\mathbf{v}}_x|_{0_+}$ depend on both the magnitude and sign of q along the edge.[¶]

We now find edge CBP solutions of Eq. **4** using the boundary condition (7) and continuity of $\phi(\mathbf{r})$. This problem is a nonlocal integro-differential equation owing to the kernel $W_q(x)$. We adopt a simplified approach, approximating $W_q(x)$ by a similar kernel $\tilde{W}_q(x)$ with the same area and second moment (22, 26): $\tilde{W}_q(x)=-\frac{e}{\kappa}\int_{-\infty}^{\infty}dk\,2qe^{ikx}/(k^2+2q^2)$. We emphasize that $\tilde{W}_q(x)$ is extended in x and captures the long-range Coulomb behavior of $W_q(x)$. Indeed, the Fourier transforms of $W_q(x)$ and $\tilde{W}_q(x)$ match for small k/q. This method has been used successfully to mimic Coulomb interactions in isolated systems (17, 28).

Crucially, the simple form of $\tilde{W}_q(x)$ above allows the integro-differential equation in Eq. **4** to be expressed as a purely differential one with $\phi_q(x)$ obeying

$$\left(\partial_x^2-2q^2\right)\phi_q^>(x)=\frac{4\pi e|q|}{\kappa}\delta n_q(x),\quad \left(\partial_x^2-2q^2\right)\phi_q^<(x)=0, \qquad [8]$$

where $\phi_q^>$ and $\phi_q^<$ are defined inside ($x\geq 0$) and outside ($x<0$) the sample, respectively. Eq. **8** yields simple ϕ profiles

$$\phi_q^<(x)=\phi_0\,e^{\gamma_0 x},\quad \phi_q^>(x)=\phi_1 e^{-\gamma_1 x}, \qquad [9]$$

where $\gamma_0=\sqrt{2}|q|$, and $\gamma_1=\sqrt{2}|q|\,\{[(\omega_{\mathbf{q}}^{\rm bulk})^2-\omega^2]/[2(\omega_{\mathbf{q}}^{\rm bulk})^2-\omega^2]\}^{1/2}$. The latter was obtained from Eqs. **4** and **7** by eliminating δn_q.

Using Eq. **9**, the boundary conditions of continuous ϕ and the jump condition (Eq. **7**) can be expressed compactly via the relation $\mathcal{S}\Phi=0$, with $\Phi=(\phi_0,\phi_1)^T$:

$$\mathcal{S}=\begin{pmatrix}1 & -1\\ \sqrt{2}|q| & \gamma_1-D\end{pmatrix},\quad D=\frac{2\gamma_1\left(\omega_q^{\rm bulk}\right)^2}{\omega^2}-\frac{q^2\tilde{\mathcal{F}}\,\mathrm{sgn}(q)}{\omega}, \qquad [10]$$

where D was obtained using Eqs. **2** and **7**, and $\tilde{F}=4\pi e^2\mathcal{F}/\kappa\hbar$. Left- and right-moving plane wave modes along the edge, $\omega_\pm^{\rm edge}$, can be identified through the zero modes of $\mathcal{S}$. We first note that for $\tilde{\mathcal{F}}=0$, solving $\det(\mathcal{S})=0$ yields degenerate nonchiral edge modes with $\omega_\pm^{\rm edge}=(2/3)^{1/2}\omega_{\mathbf{q}}^{\rm bulk}$ (17, 22, 26).

For nonzero $\tilde{\mathcal{F}}$, the zero mode solutions $\omega_\pm^{\rm edge}$ of Eq. **10** become split, yielding chiral edge plasmons (CBPs) as shown in Figs. 1 and 2. The modes $\omega_+^{\rm edge}$ and $\omega_-^{\rm edge}$ propagate as waves in opposite directions along the edge, with faster and slower speeds, respectively. Importantly, the frequencies $\omega_\pm^{\rm edge}$ depend both on q along the edge (Fig. 1*A*), as well as $\mathcal{F}$ (Fig. 2*A*). The splitting between modes grows with q and $\tilde{\mathcal{F}}$, because $\bar{\mathbf{v}}_a=e\nabla\phi\times\mathcal{F}/\hbar$ (Eq. **2**). Indeed, for small $q\tilde{\mathcal{F}}$ (so that $q\tilde{\mathcal{F}}\ll\omega_q^{\rm bulk}$), we obtain an approximate dispersion for edge CBPs as $\omega_\pm^{\rm edge}\approx(2/3)^{1/2}\omega_{\mathbf{q}}^{\rm bulk}\pm\sqrt{2}|q|\tilde{\mathcal{F}}/9+\mathcal{O}(q^2\tilde{\mathcal{F}}^2)$. As a result, we obtain the q-dependent $\Delta\omega$ in Eq. **3**. This behavior sharply contrasts with that of magnetoplasmons, which have a q-independent splitting given by the cyclotron frequency (17, 19–21, 22, 26). As a result, far larger splittings, arising from interactions, can be achieved for CBPs.

Interestingly, for large enough q and/or $\mathcal{F}$, the $\omega_+^{\rm edge}$ mode (blue line in Fig. 1 *A* and *B* and 2*A*) merges with the bulk plasmon mode $\omega_{\mathbf{q}}^{\rm bulk}$ (dashed line). As this mode merges with the bulk, its potential profile ceases to be localized along the edge.

[¶]The jump discontinuity boundary condition in Eq. **7** depends on the perpendicular velocity density at the boundary, $\bar{\mathbf{v}}_x(x=0)$. We use the subscript 0_+ in the text to emphasize that the velocity density should be evaluated on the metallic side, $x\geq 0$.

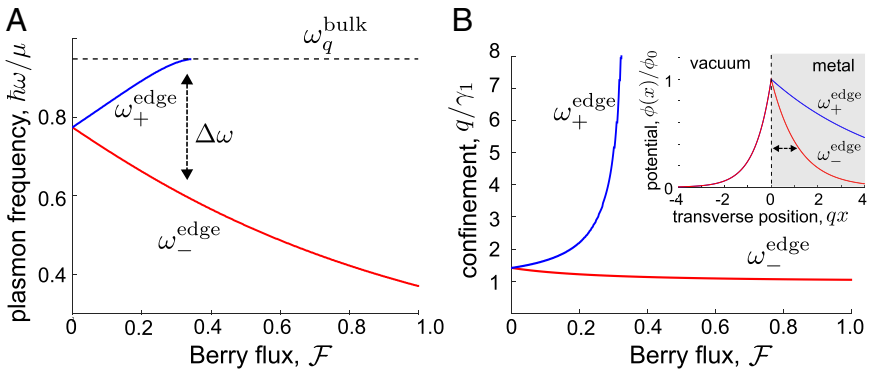

Fig. 2. CBPs at the boundary of a half plane. (*A*) The CBP frequency splitting increases with increasing Berry flux, $\mathcal{F}$. Parameter values are as in Fig. 1, but with $|q|/q_0 = 0.3$. (*B*) CBP edge-confinement length, γ_1^{-1}, of $\omega_+^{\rm edge}$ and $\omega_-^{\rm edge}$ (Eq. **9**) for increasing $\mathcal{F}$. For large $\mathcal{F}$, the confinement length of the $\omega_+^{\rm edge}$ mode diverges, indicating that it joins the bulk, whereas the $\omega_-^{\rm edge}$ mode becomes more confined to the edge. (*Inset*) Electric profile shown for $|\mathcal{F}| = 0.3$, exhibiting confinement of $\omega_\pm^{\rm edge}$ to the edge.

The disappearance of the $\omega_+^{\rm edge}$ mode is shown by a diverging confinement length of the electric potential, γ_1^{-1} (Fig. 2*B*). In contrast, $\omega_-^{\rm edge}$ stays far from the bulk dispersion, yielding a potential (and electric field) tightly confined to the edge. The threshold $\omega_{\rm th}$ above which $\omega_+^{\rm edge}$ merges with the bulk can be obtained from Eq. **10**. Setting $\omega = \omega_{\mathbf{q}}^{\rm bulk}$ in Eq. **10** yields the threshold frequency

$$\hbar\omega_{\rm th} = \frac{\hbar^2 n_0}{\sqrt{2}m|\mathcal{F}|} = 18.3\,\frac{n_0\,[\mathrm{cm}^{-2}]/10^{12}}{(m[m_e]/0.03)\times|\mathcal{F}|}\ \mathrm{meV}, \qquad [11]$$

with m_e the free electron mass. For scale we consider a plasmon mass $m \sim 0.03\ m_e$, as measured in graphene (25).

Conservation of ω and q along the edge protect the $\omega_-^{\rm edge}$ mode from coupling to bulk 2D plasmons. Scattering processes that relax q contribute to propagation losses. However, the tight edge confinement of the $\omega_-^{\rm edge}$ mode suppresses its electric field in the bulk regions (Fig. 2*B*, *Inset*), suppressing its coupling to bulk plasmons. Therefore, above the threshold $\omega_{\rm th}$ (gray region in Fig. 1*A*), the single, well-defined, $\omega_-^{\rm edge}$ mode propagates unidirectionally along the edge. When hybridized with light, it will allow for strong nonreciprocal propagation of CBP-polaritons without magnetic field (see below).

Experimental Signatures of CBPs

Strong plasmon-mediated light–matter interactions (11–13) make optics an ideal means of probing/controlling CBPs. Photon coupling to plasmons with gapless dispersion (e.g., 2D plasmons, and CBPs here) can be achieved through strategies such as gratings, and prism geometries (11). Observing unidirectional (nonreciprocal) propagation in such setups can reveal the existence of CBPs. For demonstration, we detail an alternative experimental probe: CBP-photon coupling in finite geometries, such as metallic disks, where dipolar plasmonic modes can dominate optical absorption (11, 14).

In metallic disks with finite $\mathcal{F}$, CBPs manifest as clockwise/anticlockwise moving plasmonic dipole modes (Fig. 3*A*). These modes can be described via a simple oscillator model for the motion of the dipolar CBP center of mass (COM) coordinate,[‡] $\{\mathbf{x}\}$, where $\{\cdot\}$ denotes the COM average. Here $\{\mathbf{v}_a\} \approx \mathcal{F}\ \{e\nabla\phi\} \times \hat{\mathbf{z}}$ (green arrow) gives rise to an intrinsic angular frequency ω_a of plasmons in a disk (orange arrow), which adds to (subtracts from) the plasmon frequency ω_0 to produce nondegenerate anticlockwise (clockwise) rotating modes (Fig. 3*A* and *SI Appendix*). Here we used $\mathcal{F}$ pointing to positive $\hat{\mathbf{z}}$. A bosonic analog for ultracold atomic gases is discussed in ref. 29.

With an a.c. probing electric field $\sim \mathbf{E}\, e^{i\omega t}$, the COM equations of motion are

$$\begin{aligned} \partial_t^2\{x\} + \omega_0^2\{x\} + \omega_a\partial_t\{y\} &= -eE_x\, e^{i\omega t} \\ \partial_t^2\{y\} + \omega_0^2\{y\} - \omega_a\partial_t\{x\} &= -eE_y\, e^{i\omega t}, \end{aligned} \quad \omega_a = \frac{\mathcal{F}\omega_0^2 m}{n_0\hbar}. \qquad [12]$$

Here $\omega_0(d)$ is the bare plasmon frequency in a disk of diameter d, in the absence of Berry curvature.

Writing the current density as $\mathbf{j} = en_0\,\partial_t\{\mathbf{x}\}$, we invert the COM equations of motion to obtain the optical absorption (real part of the longitudinal conductivity).[‡] As shown in Fig. 3*B*, we find a split peak structure with the dipolar CBP peaks given by the poles of Eq. **12**:

$$\omega_\pm^{\rm disk} = \sqrt{\omega_0^2 + \frac{\omega_a^2}{4}} \pm \frac{\omega_a}{2},\ \hbar\Delta\omega \equiv \mathcal{F}\hbar\omega_* \approx \frac{9\mathcal{F}}{d[\mu\mathrm{m}]}\ \mathrm{meV}, \qquad [13]$$

where $\Delta\omega = \omega_+^{\rm disk} - \omega_-^{\rm disk} = \omega_a$ and $\hbar\omega_* = \omega_0^2 m/n_0$. On the right side, we estimated $\omega_0^2 \approx 2\pi e^2 n_0|\mathbf{q}|/m$, with $|\mathbf{q}| \approx 1/d$ (approximating the lowest lying plasmonic excitation in a disk).[#] Here we used $\kappa = 1$. Importantly, $\Delta\omega$ depends on the disk size, d, a unique property of CBPs.

The tunable optical absorption split peak structure (via $\mathcal{F}$ and d) in the absence of an applied magnetic field gives a clear experimental signature of CBPs. In plotting Fig. 3*B*, we included the damping rate phenomenologically via $\partial_t^2 \to \partial_t^2 + \Gamma\partial_t$, yielding a Lorentzian lineshape with its half-width determined by Γ. Split peaks are clearly visible when $\Delta\omega \gtrsim \Gamma$, yielding peaks at $\omega_\pm^{\rm disk}$. To give a sense of scale, we note a typical value $\hbar\Gamma \sim$ few meV (30), where $\hbar\Gamma \approx 4$ meV was measured in graphene disks. Using $\Gamma/\omega_* = 0.25$ and taking $\mathcal{F} = 1$, clearly resolved $\omega_\pm^{\rm disk}$ peaks can be resolved for disk sizes $d \lesssim 1$ μm (Fig. 3*B*).

CBPs in Anomalous Hall Materials

We now discuss materials where CBPs can be realized. We predict that metallic systems with nonvanishing $\mathcal{F}$ will generically host CBPs. Finite $\mathcal{F}$ requires broken time reversal symmetry and may arise in magnetically ordered systems or out-of-equilibrium nonmagnetic systems (see below). The former includes magnetically doped semiconducting quantum wells (see ref. 31, where $\mathcal{F} \approx 1/2$ was predicted) and topological insulators (3–6).

[#]Comparing this estimate to plasmon frequencies obtained in graphene disks (30), we obtain zero field plasmon frequencies in the disk geometry to within a factor of unity. Using parameters reported in ref. 30, our estimate yields $\hbar\omega_0 \approx \sqrt{2\pi e^2 n_0/(md)} \approx 24$ meV for a disk of $d = 3$ μm and reported doping $\mu = -0.54$ eV. Ref. 30 observed a zero field plasmon resonance at $\omega_0 = 130\ \mathrm{cm}^{-1} = 16$ meV.

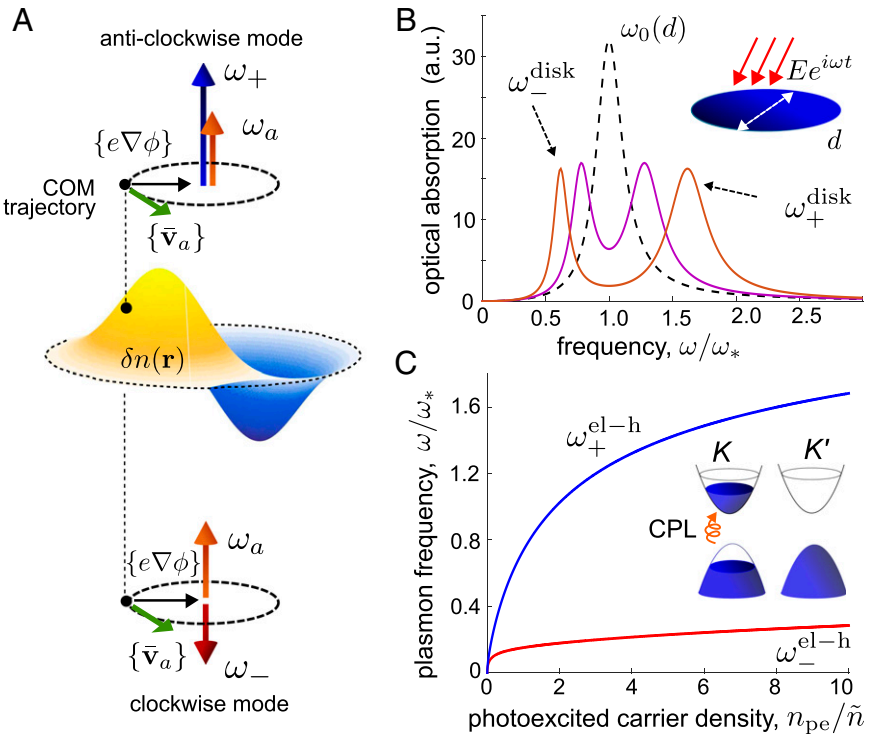

Fig. 3. CBPs in a disk and in valley polarized gapped Dirac systems. (*A*) Illustration of CBPs in a disk, showing anticlockwise/clockwise rotating dipole modes. The mode splitting arises from the intrinsic angular frequency, ω_a, induced by the combination of $\mathcal{F}$ and the self-induced electric field. (*B*) Optical absorption split peaks for dipolar CBPs in a disk (*A*) obtained by inverting Eq. **12** for $\mathcal{F}=0, 0.5, 1.0$ (dashed black, purple, orange). Smaller disk sizes and/or larger $\mathcal{F}$ produce larger splittings (Eq. **13**). Parameter values: $\omega_0/\omega_*=1$ and $\Gamma/\omega_*=0.25$. (*C*) CBP dipole modes for valley polarized gapped Dirac systems, with $n_K=n_{\rm pe}$, and $n_{K'}=0$. The characteristic density is $\tilde{n}=\Delta^2/4\pi v_F^2\hbar^2$. (*Inset*) Valley polarization may be induced by above-gap circularly polarized light.

As a concrete example, we examine the magnetically doped topological insulator chromium doped thin-film $(Bi,Sb)_2Te_3$, which was recently experimentally realized (5). When moderately doped with electrons or holes, we estimate that $\mathcal{F}\sim 1$ can be achieved based on the measured anomalous Hall conductivity $\sigma_{xy}^{B=0}\lesssim e^2/h$ (5). These values yield a large splitting $\hbar\Delta\omega\approx 10-100$ meV for short wavelength plasmons (Eqs. **3** and **13**). When probed in the disk geometry, we predict this system will yield two split absorption peaks in the absence of magnetic field.

On-Demand CBPs in Nonmagnetic Materials

Intriguingly, finite $\mathcal{F}$ can also be achieved in nonmagnetic materials, without an applied magnetic field. This class includes, for example, gapped Dirac materials where inversion symmetry is broken. In these, a valley polarization (Fig. 3*C*, *Inset*) can be induced by circularly polarized light (32), yielding an anomalous Hall effect that has recently been observed (7).

Can CBPs exist in photoexcited systems? To analyze this, we focus on nominally time reversal invariant gapped Dirac materials. We model the valley dependent $\mathcal{F}$ as (33) $\mathcal{F}_{K,K'}=\tau_z N_s\{\tilde{n}^{1/2}/[2(n_{K,K'}+\tilde{n})^{1/2}]\}$ sgn Δ, where $n_{K,K'}$ are the valley carrier densities, $\tau_z=\mp$ for the K,K' valleys, $N_s=2$ is the spin degeneracy, and $\tilde{n}=\Delta^2/4\pi v_F^2\hbar^2$ gives a characteristic density scale. The bandgap is $2|\Delta|$. When $n_K=n_{K'}$ is in equilibrium, the total flux $\mathcal{F}=\mathcal{F}_K+\mathcal{F}_{K'}$ vanishes.

Interestingly, when the system is pushed out of equilibrium, e.g., by circularly polarized light, the populations in the valleys may become imbalanced, $n_K\neq n_{K'}$ (32) (Fig. 3*C*, *Inset*).[‡] As a result, the net Berry flux for the entire electronic system (summed over both valleys) is nonzero, yielding $\mathcal{F}_{\rm pe}\neq 0$. We analyze the collective modes of the photoexcited electron-hole system in the disk geometry following Eq. **12**, accounting for the mutually attracting electron and hole populations and using $\mathcal{F}=\mathcal{F}_{\rm pe}$. This analysis yields two chiral CBP modes: $\omega_\pm^{\rm el-h}=\sqrt{\omega_a^2+2\omega_0^2}\pm\omega_a$ (*SI Appendix*). Estimating ω_0 as in the text below Eq. **13**, we obtain the $\omega_\pm^{\rm el-h}$ curves in Fig. 3*C* with ω_* given by Eq. **13**. The frequencies of both modes vanish at zero photoexcited carrier density, $n_{\rm pe}$. The mode splitting increases with $n_{\rm pe}$ and can reach sizable values for $n_{\rm pe}\gtrsim\tilde{n}$, reflecting $\mathcal{F}_{\rm pe}$ pumping.

Large splittings require $n_{\rm pe}\gtrsim\tilde{n}$. The large gaps $\Delta\gtrsim 1$ eV of many transition metal dichalcogenides (7, 34, 35) yield large characteristic densities requirements, $\tilde{n}\gtrsim 10^{13}$ cm^{-2}. In contrast, other gapped Dirac materials such as G/hBN (36–38) and dual-gated bilayer graphene (39) possess $\Delta\approx 10-200$ meV, yielding significantly smaller and more favorable $\tilde{n}$. These materials possess valley-selective optical selection rules (32),[‡] and present an ideal venue to achieve maximal $\mathcal{F}=1$ (and large $\Delta\omega$), even with relatively weak pump fluence.[||]

A further promising strategy to achieve large CBP splittings is to stack m layers of gapped Dirac materials on top of each other, with no tunnel coupling between the layers. Stacking achieves (*i*) larger photo-excited carrier densities due to the increased absorption and (*2*) a larger maximal Berry flux (when $n_{\rm pe}\gg\tilde{n}$) and, hence, larger CBP splittings; the maximal Berry flux is $\mathcal{F}_{\rm max}=m\mathcal{F}_{\rm single}$. In such a structure, the long-range Coulomb interaction allows the photoexcited densities in different layers to oscillate collectively.

Conclusion

CBPs are robust collective excitations of metallic systems, arising from two simple ingredients: Berry flux and interactions. Our

[||]Note that the (neutral) excitons that may form in some large-gap materials feel zero net Berry curvature (43) and to first approximation do not contribute to CBPs.

analysis indicates that CBPs survive for both weak and strong interactions. As a result, we conclude that CBPs are generic in metallic anomalous Hall phases, including out-of-equilibrium states where finite $\mathcal{F}$ emerges from driving (e.g., in optically pumped valley polarized gapped Dirac materials). Indeed, this feature allows CBPs to be used for all-optical diagnostics of anomalous Hall and topological phases, as well as pumped or periodically driven systems (40, 41). Optical probes of the latter are particularly appealing because transport measurements require contacts that often complicate and destroy the novel electron distributions and coherences of driven systems.

Perhaps the most appealing prospect is coupling CBPs with light for subwavelength and strong nonreciprocal propagation. Exhibiting a single chiral mode at large q (large splitting and large frequency), precisely where plasmons give large compression of optical mode volume, hybrid CBP-polaritons are strongly nonreciprocal (10). As we propose, CBP mediated unidirectional waveguides can be realized in readily available nonmagnetic materials (e.g., the van der Waals material class). CBP-based nonreciprocity, if realized experimentally, stands to play a vital role in the miniaturization of optical components that are magnetic field free.

Note Added in Proof. During the review of our manuscript, a related work on CBPs in photoexcited gapped Dirac systems appeared (44).

ACKNOWLEDGMENTS. We thank J. Alicea, J. Eisenstein, M. Kats, L. Levitov, M. Schecter, and B. Skinner for useful conversations. J.C.W.S. acknowledges support from the Walter Burke Institute for Theoretical Physics as part of a Burke fellowship at California Institute of Technology. M.S.R. acknowledges support from the Villum Foundation and the People Programme (Marie Curie Actions) of the European Union's Seventh Framework Programme (FP7/2007-2013) under Research Executive Agency Grant PIIF-GA-2013-627838.

1. Nagaosa N, Sinova J, Onoda S, MacDonald AH, Ong NP (2010) Anomalous Hall effect. *Rev Mod Phys* 82(2):1529–1592.
2. Haldane FDM (1988) Model for a quantum Hall effect without Landau levels: Condensed-matter realization of the "parity anomaly". *Phys Rev Lett* 61(18):2015–2018.
3. Yu R, et al. (2010) Quantized anomalous Hall effect in magnetic topological insulators. *Science* 329(5987):61–64.
4. Nomura K, Nagaosa N (2011) Surface-quantized anomalous Hall current and the magnetoelectric effect in magnetically disordered topological insulators. *Phys Rev Lett* 106(16):166802.
5. Chang C-Z, et al. (2013) Experimental observation of the quantum anomalous Hall effect in a magnetic topological insulator. *Science* 340(6129):167–170.
6. Wang Q-Z, et al. (2014) Quantum anomalous Hall effect in magnetically doped InAs/GaSb quantum wells. *Phys Rev Lett* 113(14):147201.
7. Mak KF, McGill KL, Park J, McEuen PL (2014) Valleytronics. The valley Hall effect in MoS_2 transistors. *Science* 344(6191):1489–1492.
8. Xiao D, Meng MC, Niu Q (2010) Berry phase effects on electronic properties. *Rev Mod Phys* 82(3):1959–2007.
9. Hasan MZ, Kane CL (2010) Colloquium: Topological insulators. *Rev Mod Phys* 82(4): 3045–3067.
10. Jalas D, et al. (2013) What is—and is not—an optical isolator. *Nat Photonics* 7(8): 579–582.
11. Barnes WL, Dereux A, Ebbesen TW (2003) Surface plasmon subwavelength optics. *Nature* 424(6950):824–830.
12. Tame MS, et al. (2013) Quantum plasmonics. *Nat Phys* 9(6):329–340.
13. Grigorenko AN, Polini M, Novoselov KS (2012) Graphene plasmonics. *Nat Photonics* 6(11):749–758.
14. Allen SJ, Störmer HL, Hwang JCM (1983) Dimensional resonance of the two-dimensional electron gas in selectively doped GaAs/A_1GaAs heterostructures. *Phys Rev B* 28(8):4875.
15. Theis TN (1980) Plasmons in inversion layers, *Surf Sci* 98(1):515–532.
16. Heitman D (1986) Two-dimensional plasmons in homogeneous and laterally microstructured space charge layers. *Surf Sci* 170(1):332–345.
17. Mast DB, Dahm AJ, Fetter AL (1985) Observation of bulk and edge magnetoplasmons in a two-dimensional electron fluid. *Phys Rev Lett* 54(15):1706–1709.
18. Glattli DC, Andrei EY, Deville G, Poitrenaud J, Williams FIB (1985) Dynamical Hall effect in a two-dimensional classical plasma. *Phys Rev Lett* 54(15):1710–1713.
19. Kohn W (1961) Cyclotron resonance and de Haas-van Alphen oscillations of an interacting electron gas. *Phys Rev* 123(4):1242.
20. Brey L, Johnson NF, Halperin BI (1989) Optical and magneto-optical absorption in parabolic quantum wells. *Phys Rev B* 40(15):10647–10649.
21. Maksym PA, Chakraborty T (1990) Quantum dots in a magnetic field: Role of electron-electron interactions. *Phys Rev Lett* 65(1):108–111.
22. Fetter AL (1985) Edge magnetoplasmons in a bounded two-dimensional electron fluid. *Phys Rev B Condens Matter* 32(12):7676–7684.
23. Lifshitz EM, Pitaevskii LP (1981) *Physical Kinetics* (Butterworth-Heinemann, Oxford, UK).
24. Giuliani GF, Vignale G (2005) *Quantum Theory of the Electron Liquid* (Cambridge Univ Press, Cambridge, UK).
25. Yoon H, et al. (2014) Measurement of collective dynamical mass of Dirac fermions in graphene. *Nat Nanotechnol* 9(8):594–599.
26. Fetter AL (1986) Edge magnetoplasmons in a two-dimensional electron fluid confined to a half-plane. *Phys Rev B Condens Matter* 33(6):3717–3723.
27. Volkov VA, Mikhailov SA (1988) Edge magnetoplasmons: Low frequency weakly damped excitations in inhomogeneous two-dimensional electron systems. *Sov Phys JETP* 67(8):1639–1653.
28. Wang W, Apell P, Kinaret J (2011) Edge plasmons in graphene nanostructures. *Phys Rev B* 84(8):085423.
29. Price HM, Cooper NR (2013) Effects of Berry curvature on the collective modes of ultracold gases. *Phys Rev Lett* 111(22):220407.
30. Yan H, et al. (2012) Infrared spectroscopy of tunable Dirac terahertz magneto-plasmons in graphene. *Nano Lett* 12(7):3766–3771.
31. Culcer D, MacDonald AH, Niu Q (2003) Anomalous Hall effect in paramagnetic two-dimensional systems. *Phys Rev B* 68(4):045327.
32. Yao W, Xiao D, Niu Q (2008) Valley-dependent optoelectronics from inversion symmetry breaking. *Phys Rev B* 77(23):235406.
33. Lensky YD, Song JCW, Samutpraphoot P, Levitov LS (2015) Topological Valley Currents in Gapped Dirac Materials. *Phys Rev Lett* 114(25):256601.
34. Jones AM, et al. (2013) Optical generation of excitonic valley coherence in monolayer WSe2. *Nat Nanotechnol* 8(9):634–638.
35. Ruppert C, Aslan OB, Heinz TF (2014) Optical properties and band gap of single- and few-layer MoTe2 crystals.$_2$ *Nano Lett* 14(11):6231–6236.
36. Hunt B, et al. (2013) Massive Dirac fermions and Hofstadter butterfly in a van der Waals heterostructure. *Science* 340(6139):1427–1430.
37. Woods CR, et al. (2014) Commensurate-incommensurate transition in graphene on hexagonal boron nitride. *Nat Phys* 10(6):451–456.
38. Gorbachev RV, et al. (2014) Detecting topological currents in graphene superlattices. *Science* 346(6208):448–451.
39. Zhang Y, et al. (2009) Direct observation of a widely tunable bandgap in bilayer graphene. *Nature* 459(7248):820–823.
40. Yao W, MacDonald AH, Niu Q (2007) Optical control of topological quantum transport in semiconductors. *Phys Rev Lett* 99(4):047401.
41. Kitagawa T, Oka T, Brataas A, Fu L, Demler E (2011) Transport properties of non-equilibrium systems under the application of light: Photoinduced quantum Hall insulators without Landau levels. *Phys Rev B* 84(23):235108.
42. Henriksen EA, et al. (2010) Interaction-induced shift of the cyclotron resonance of graphene using infrared spectroscopy. *Phys Rev Lett* 104(6):067404.
43. Yu H, Liu G-B, Gong P, Xu X, Yao W (2014) Dirac cones and Dirac saddle points of bright excitons in monolayer transition metal dichalcogenides. *Nat Commun* 5:3876.
44. Kumar A, et al. (2016) Chiral plasmon in gapped Dirac systems. *Phys Rev B* 93:041413.